Mechanical investigation of weak regions in a wound oxide-oxide ceramic matrix composite

Viacheslav Vasechko*, Ferdinand Flucht, Nils Rahner

German Aerospace Center (DLR), Institute of Materials Research, D-51147 Cologne, Germany

Abstract: The main aim of the investigation was to quantify the influence of production-related cross-lines on static mechanical properties (tensile, flexural and shear) of an oxide-oxide CMC as a comparison between specimens with cross-lines and specimens without cross-lines in tested regions. Investigated material was a weak-matrix oxide-oxide CMC (WHIPOX™) made of Nextel™ 610 fibers (3000 denier) and alumina matrix with a special winding pattern. Mechanical tests at room temperature revealed that cross-lines were local weak regions in a wound component. Spatial separation of the cross-line within the composite (2 mm shift from layer to layer) did not improve the negative influence of the cross-lines on mechanical properties. Fractographic investigations revealed that cross-lines acted as a trigger of material failure.

Keywords: ceramic matrix composite; mechanical properties; strength; failure analysis; fractography.

*corresponding author: viacheslav.vasechko@dlr.de

I. Introduction

Oxide-oxide ceramic matrix composites (CMCs) are developed as candidate materials for turbine engine, combustion chamber and other industrial applications due to their promising high-temperature performance[1,2]. This fact makes them more advantageous in comparison to common nickel-based superalloys[3] and non-oxide fiber/non-oxide matrix ceramic matrix composites[4,5]. However, high-temperature vulnerability of oxide-oxide CMCs in steam still remains an issue for future turbine applications[6]. Low specific weight is another advantage of porous oxide-oxide CMCs making it attractive for lightweight application in aerospace industry[7].

Application of a material as a structural component is directly connected to its reliability. The material should possess mechanical properties sufficient to sustain application-related loads at corresponding conditions. Therefore, it is important to understand material behavior (failure mechanisms and origins) to improve its mechanical properties (increase of an absolute value, decrease of a property scatter) and widen its potential applications as a structural component. This could be performed in a loop of material production – mechanical testing –fractography of tested specimens.

Different approaches have been tried to investigate mechanical performance of all-oxide CMCs: starting from a single filament testing[8], going to mini-composites (infiltrated fiber bundle)[9] and ending up with large-scale composite products[10,11,12].

The problem of mini-composites is their simplification of the application-related composite microstructure that results in a limited usage of the obtained data for the prediction of CMC behavior in real components. Another limiting issue of matrix-infiltrated fiber bundles is their manufacturing reproducibility that increases the scatter of obtained data and complicates the interpretation of results. At the same time application-relevant CMC components (plates, pipes, etc.) have a complicated structure making their mechanical performance dependent on numerous factors (CMC architecture, fiber roving parameters, ceramic slurry parameters, etc.) which are impossible to separate for a systematic investigation via mechanical testing. Therefore, there is a need of a simplified reproducible application-sized, e.g. plate-sized, ceramic matrix composite in order to reduce its microstructural complexity. This microstructural simplification would help to understand the mechanical behavior of an oxide-oxide CMC giving a hint to an increase of its mechanical properties.

Up to now several production routes are established for oxide-oxide CMC, e.g. prepreg-based, winding-based[13]. Various production routes end-up in numerous patterns and local architectures of CMCs (e.g. weaving patterns of fabrics for prepreg-based production, winding pattern of fiber bundle for winding technique). In this study a wound CMC material was produced with a special winding pattern to have regions with a simplified reproducible CMC architecture.

Mechanical properties were already assessed in previous investigations of all-oxide CMCs. Some publications contain fundamental knowledge of CMC

mechanical behavior with statistically limited data[10,11,12]. Other works quantified mechanical properties based on numerous experiments per data point[14,15]. An additional highlight of current investigation is the large amount of tested specimens (between 6 and 15 for a data point) resulting in higher reliability of the presented data.

II. Experimental procedure

The oxide-oxide ceramic matrix composite (WHIPOX™) tested in this study was manufactured via winding process[7]. Production process started with infiltration of a Nextel™ 610 roving (3000 denier) with water-based alumina slurry. The slurry was prepared from Pural SB manufactured by Sasol. As-delivered powder was calcinated and milled to d_{50} = 0.5 µm (measured with Mastersizer MS2000 from Malvern). The infiltrated fiber bundle was wound on a mandrel with 45° angle resulting in architecture typical for winding process: intersection of a forward- and backward-wound infiltrated fiber roving as demonstrated in Fig. 1. The repetition of this forward-backward winding pattern over the mandrel resulted in a CMC layer covering 100% of the mandrel surface (Fig. 1) with cylindrical regions without cross-lines (laminate) and cross-lines themselves.

Every wound CMC layer consisted of 2 sub-layers (Fig. 1) forming a 2D-composite with a thickness of 0.3 mm. In this investigation every plate contained 20 layers of the 2D composite to reach a green-body thickness of approximately 6 mm. A special optimized winding pattern was used for current investigation to have a

maximum distance between the neighboring cross-lines (approximately 170 mm). After the winding process the wound body was cut along the winding axis, taken off the mandrel and flattened in a plate. After forming procedure every plate was left to dry at room temperature. After the drying stage the plates were sintered at 1300 °C for 1 hour. After sintering process every plate was plan-parallel ground down to 3.0 mm thickness leading to a reduction of layers in the plate to 10 or 11 (depending on plate curvature after sintering process). The grinding procedure was required for a constant plate thickness in order to avoid an unexpected stress development in mechanically tested specimens under loading conditions.

This kind of architecture (170 mm between cross-lines) gave a possibility to investigate 2 types of specimens: without cross-lines (so-called “laminate”) and with cross-lines as it is demonstrated in Fig. 2.

A variation in cross-line region was performed as an attempt to reduce a possible negative influence of stacked cross-lines on the mechanical properties: the cross-line was shifted from layer to layer by 2 mm to separate the cross-lines from each other. This resulted in 2 sub-types of uniaxial tensile specimens with cross-lines: stacked cross-lines (stCL) and shifted cross-lines (shCL).

The specimens were prepared and tested with 2 fiber orientations: +45°/-45° and 0°/90° with respect to the loading direction.

The regions with and without cross-lines had notably different mesostructure as it is demonstrated in Fig. 3. Regions with cross-lines contained large voids with

missing ceramic matrix, whereas regions without cross-lines were free of large defects.

Several CMC plates were produced for mechanical experiments (product number W1600, W1601, W1602, W1619 and W1639) to obtain a specimen batch for every investigated aspect. After material production relevant material properties were assessed: density = 3.00±0.07 g/cm3, open porosity = 20.8±3.6 % (measured according to ISO 5017:2013), fiber volume fraction (FVC) = 35.8±4.0 %. Due to present fluctuations in fiber volume fraction (relevant for absolute values of mechanical properties) every value of investigated aspect was compared to a reference value of the current material (from laminate region) to calculate a relative decrease of the property independent from batch quality fluctuations. Fiber volume fraction difference between regions with and without cross-lines was not possible to quantify due to a fact that fiber volume fraction could be calculated only for the entire plate (based on mass control of the used raw materials, final product and product residuals).

Uniaxial tensile properties were assessed with Instron® 4505 testing frame at room temperature. Specimen dimensions were 140 × 20 × 3 mm^3 (tested region: 40 × 10 × 3 mm^3). Uniaxial tensile specimens were cut out of a plate via waterjet-cutting. Every tensile specimen was tested with 1 mm/min displacement rate. A load cell of 10 kN was used for force measurements. Material displacement in the testing region (l_0 = 40 mm) was measured with a laser extensometer (parallel scanner P-130, Fiedler Optoelektronik GmbH) with a 1 mm step between 1 mm wide

measurement stripes. Strain calculations were performed for the entire tested region length, i.e. between stripe 1 and stripe 21.

Flexural properties were assessed via 4-point bending experiments with Zwick Roell® UTS 10 testing frame at room temperature. Specimen dimensions were 85 × 10 × 3 mm^3. The displacement rate was 2 mm/min. A load cell of 2.5 kN was used for force measurements. Distance between the loading rolls was 20 mm and 80 mm between the supporting ones. Specimen deflection was measured in the middle of tension-loaded side of the bending specimen with inductive probe Millitron 1310.

Interlaminar shear strength was assessed via double-notch compression experiments with Zwick Roell® UTS 10 testing frame at room temperature. Specimen geometry was 30 × 15 × 3 mm^3. Distance between the notches was 10 mm resulting in a sheared area of 10 × 15 mm^2. The displacement rate was 0.5 mm/min. A load cell of 2.5 kN was used for force measurements. Specimen deformation was not measured (only set-up displacement was available).

Digital stereo microscope Keyence VHX-1000 was used for fractographic inspections of tested specimens.

Data obtained in uniaxial tensile experiments were analyzed according to ASTM C1275-16 standard. Following parameters were extracted from the stress-strain curves: tensile strength S_u, strain at tensile strength ε_u. Tensile strength S_u was defined as stress at the point of maximum load before material failure. In this

investigation the failure criterion was defined as 5% drop of current tensile stress during experiment (referred to the previous point on a stress-strain curve) at stresses >50 MPa, 5% increase of the current strain value (referred to the previous point on a stress-strain curve) at strains > 0.05% in tested region.

The results of uniaxial tensile experiments are presented in the form of fracture point (mean tensile strength S_u and mean strain at tensile strength ε_u for a specimen batch) in stress-strain coordinate system.

Experimental data obtained via 4-point bending tests were analyzed according ASTM C1341-13. The parameters used to describe material behavior in flexural tests were mean flexure stress σ, mean flexure strain ε. A modification of stress and strain calculations was suited to current set-up configuration (20 mm between loading rolls and 80 mm between supporting rolls):

$$\sigma = \frac{9}{8} \cdot \frac{P \cdot L}{b \cdot d^2} \quad (1)$$

$$\varepsilon = \frac{576}{117} \cdot \frac{D \cdot d}{L^2} \quad (2)$$

An important remark should be done to strain calculation: the deflection was measured with an inductive probe under a specimen middle point. The contribution of the set-up to the measured specimen deflection was neglected.

Interlaminar shear strength was measured via double-notch compression test and calculated as defined in ASTM C1292-16.

III. Results and discussion

Uniaxial tensile tests were performed with specimens of 2 fiber orientations with respect to tension direction: 0°/90° (50 vol. % of fibers oriented in tension direction and 50 vol. % perpendicular to tension direction) and +45°/-45° (50 vol. % of fibers oriented at +45° with respect to tension direction and 50 vol. % at -45° with respect to tension direction).

The results of 0°/90° fiber-oriented specimens represented fiber-dominated material behavior, whereas the +45°/-45° fiber-oriented ones included both fiber and matrix contributions to the mechanical behavior.

An example of tensile stress-strain curves of specimens tested in this work is demonstrated in Fig. 4. Specimens with 0°/90° fiber orientation (4VV29F and 4VV22F) demonstrated pure elastic behavior up to fracture (point of a maximum load), whereas the specimens with +45°/-45° fiber orientation revealed quasi-plastic behavior. Both curve types are already well-known for CMCs[14,16,17,18,19]. Another important feature was observed during tensile tests: lower tensile strength values for specimens with cross-lines (specimen 4VV22F and 4VV26E) in comparison to specimens without cross-lines from laminate region (4VV29F and 4VV2E, respectively). Therefore, more specimens were produced and tested for a statistical confirmation of these observations. An additional feature of the investigation campaign was an attempt to improve the mechanical performance of the material regions with cross-lines via a 2mm horizontal shift of the cross-lines from layer to layer. Therefore, 3 sorts of specimens were tested in tension: without cross-lines (L), with stacked cross-lines (stCL) and with shifted cross-lines (shCL).

The results are presented in Fig. 5 in terms of mean value with standard deviation. Summarized tensile properties are shown in Table 1.

First plate W1600 was used for the investigation of +45°/-45° fiber-oriented specimens with stacked cross-lines. 13 samples without cross-lines (W1600 (L +-45), 13 specimens) were tested as a comparison baseline: 114±8 MPa tensile strength and 0.218±0.024 % of strain at tensile strength. The following specimens with stacked cross-lines (W1600 (stCL+-45), 12 specimens) resulted in 103±9 MPa tensile strength and 0.176±0.022 % of strain at tensile strength. Therefore, the influence of the stacked cross-lines was quantified as -10% of tensile strength and -19% of strain at tensile strength.

A similar investigation was performed with the second plate W1617: the influence of stacked cross-lines on the tensile properties in 0°/90° fiber orientation was quantified. The reference specimens (W1617 (L 0/90), 9 specimens): 192±21 MPa tensile strength and 0.177±0.024 % of strain at tensile strength. Tensile specimens with stacked cross-lines (W1617 (stCL 0/90), 9 specimens) had 162±16 MPa of tensile strength and 0.166±0.017 % of strain at tensile strength. Finally, material regions with stacked cross-lines had lower tensile strength (-16 % for stacked cross-lines) and lower strain at tensile strength (-6%) in comparison to regions without cross-lines (laminate). These data demonstrated that stacked cross-line regions were locally weak regions within the material having lower tensile strength, strain at tensile strength in comparison to regions without cross-lines.

Fractographic investigations of the tensile specimens were performed to reveal more issues of failure origins. Fundamental difference in failure mode was observed between 0°/90° and +45°/-45° fiber-oriented specimens. An example is illustrated in Fig. 6. The specimen with +45°/-45° fiber orientation (Fig. 6a and 6b) revealed a matrix shear failure under uniaxial tensile load. Shear stress component presented in the material during the loading exceeded the shear strength value of the weak porous matrix and resulted in a specimen failure. The specimen with 0°/90° fiber orientation (Fig. 6c and 6d) demonstrated a fiber tensile failure with interlaminar delamination.

Tensile fiber failure for 0°/90° fiber-oriented specimens with cross-lines (Fig. 7) is similar to specimens without cross-lines: tensile fiber failure combined with interlaminar delamination. This could be seen comparing Fig. 6c and 6d (without cross-lines) with Fig. 7c and 7d (with cross-lines). One reason for failure strength difference (192 MPa and 162 MPa) could be poor infiltration of the fiber boundles in the cross-line region (Fig. 3b and 3c). This poor infiltration should negatively affect local stress distribution: high local stresses for bundles without connection to neighboring bundles. A similar effect is well-known as porosity effect on local stress distribution where local stresses could reach up to 3 times of nominal stress value[20,21].

New developments at DLR raised up a need to compare current material with state-of-the-art oxide/oxide CMCs. A comprehensive study of available materials was performed by Volkmann et al.[22]. Currently investigated material demonstrated

tensile properties in 0°/90° fiber orientation (196 MPa tensile strength as average of W1601 and W1617) close to already known similar materials based on N610 fibers[3,22,23,24,25]. Higher values (230 MPa tensile strength) were previously achieved by UCSB[26]. This could be associated with a higher fiber volume fraction (FVF = 39 vol.%) of UCSB material. COI ceramics developed a composite with extraordinary properties (366 MPa tensile strength) at ambient temperature with a sol-gel infiltration technique and resulting 51 vol.% FVF[27]. Another excellent material (~300 MPa tensile strength) was produced via sol-gel infiltration technique[28]. This could be explained with 48 vol.% FVF as in case of COI material. In conclusion, current WHIPOX material could be placed in a middle field of up-to-date oxide/oxide CMCs. Nevertheless, a notable improvement was achieved at DLR in past years increasing the tensile strength from 110 MPa[29] to 192 MPa measured in this work. Current material was produced with the same cost-effective slurry infiltration technique.

As mentioned before, an attempt to improve the mechanical performance of the regions with cross-lines was performed: the cross-lines were shifted by 2 mm from layer to layer. For this investigation purpose plates W1602 and W1601 were manufactured and tested. The first one (W1602) served for the quantification in +45°/-45° fiber orientation, while the second one (W1601) for the 0°/90° fiber orientation. Fracture data points are presented along with the laminate (L, material without cross-lines) reference points in Fig. 5. The corresponding values are given in Table 1.

For +45°/-45° fiber-oriented specimens with shifted cross-lines (W1602 (shCL +-45), 9 specimens) the decrease was -13 % for tensile strength and -15 % for strain at tensile strength in comparison to laminate region (W1602 (L +-45), 15 specimens).

W1601 was produced to investigate the influence of shifted cross-lines on the tensile properties in 0°/90° fiber orientation. These tensile tests (W1601 (shCL 0/90), 9 specimens) demonstrated that material regions with shifted cross-lines had lower tensile strength (-18 %) and lower strain at tensile strength (-15%) in comparison to material without cross-lines (W1601 (L 0/90), 10 specimens).

Fractographic investigation of tensile specimens with shifted cross-lines were identical to ones with stacked cross-lines and confirmed the statement of their local mechanical weakness: all fracture surfaces were in contact with a cross-line. Cross-lines acted as a trigger for specimen failure.

An attempt to improve the mechanical performance of weak cross-line regions via shift of the cross-line by 2 mm from layer to layer did not succeed: the decrease of tensile strength and strain at tensile strength remained at the same level. Therefore, further experiments (4-point bending and double-notch compression) were performed only for material with stacked cross-lines.

W1639 was produced to investigate the influence of stacked cross-lines on flexural properties. First 4-point bending experiments were performed with +45°/-45° fiber-

oriented specimens. The cross-lines were positioned between the loading rolls. Fracture data are presented in Fig. 8. Absolute values are listed in Table 2.

Mechanical properties for the specimens with stacked cross-lines (stCL +-45) were lower than of ones without cross-lines (L +-45): -10 % of flexural strength, -15% of strain at flexural strength. The same bending experiment was performed for 0°/90° fiber-oriented 4-point bending specimens from W1639. Mechanical properties for the specimens with cross-lines (stCL 0/90) were lower than of specimens without cross-lines (L 0/90): -22 % of flexural strength, -13% of strain at flexural strength.

Fractographic investigations of bending specimens without cross-lines revealed multiple interlaminar delaminations of tested specimens as it is demonstrated in Fig. 9. Fracture lines occurred on the tensile-loaded surfaces of the specimens were the delaminations coming out on the surface (grinding process of the specimens led to interruptions in surface sub-layers). This interlaminar delamination pattern was observed for both +45°/-45° and 0°/90° fiber-orientated specimens. In contrast to tensile specimens (Fig. 6) no tensile failure of fibers was observed for 0°/90° fiber-orientated bending specimens. The same fracture pattern (interlaminar delamination) was detected after bending experiments of specimens with stacked cross-lines.

Basing on the flexural properties and fractographic investigations of the bending specimens it was concluded that cross-lines decreased local flexural properties of the wound ceramic matrix composite.

Previous microscopic investigations of the cross-lines (Fig. 3) demonstrated that these regions were poorly infiltrated with ceramic slurry leading to voids in the CMC microstructure. This fact should be critical for matrix-dominated mechanical properties in the cross-line regions. One of the possibilities to confirm this statement was interlaminar shear testing of the specimens with and without cross-lines. Therefore, double-notch compression tests of specimens without cross-lines and specimens with stacked cross-lines were carried out. The values are presented in Table 3.

A remarkable decrease (-28%) of interlaminar shear strength was observed for specimens with stacked cross-lines (5.3±0.6 MPa, 10 specimens) in comparison to ones without cross-lines (7.4±0.2 MPa, 10 specimens) for +45°/-45° fiber orientation. A similar investigation was performed for 0°/90° fiber-oriented material. Mechanical properties for the specimens with stacked cross-lines (9.7±1.0 MPa, 6 specimens) were lower than of without cross-lines (13.5±1.4 MPa, 6 specimens): -28 % of interlaminar shear strength. The decrease of interlaminar shear strength due to presence of stacked cross-lines was independent of fiber orientation. The difference in absolute values for +45°/-45° and 0°/90° fiber-oriented specimens (7.4±0.2 MPa and 13.5±1.4 MPa, respectively) could be referred to scatter in material quality. Fractographic investigations of tested specimens demonstrated the same failure modus (interlaminar shear) for all tested specimens (Fig. 10)

IV. Summary

All tests performed within this investigation campaign indicated that cross-lines negatively affected tensile, flexural and shear properties of WHIPOX at room temperature. Fractographic investigations confirmed this statement with a fact that cross-lines acted as failure trigger.

An attempt to improve mechanical properties of the oxide-oxide composite via spatial shift of cross-lines from layer to layer did not succeed (variations of absolute value were within standard deviation). This fact was proved via uniaxial tensile experiments.

These mechanical tests revealed an important manufacturing issue: winding of oxide-oxide CMC should be performed with minimal amount of cross-lines in a final component, i.e. winding pattern with the largest possible rhomb unit, to have less weak zones (cross-lines) in a final component. An additional condition for further application would be the placement of a component region with a cross-line in a zone with lower mechanical loads.

This investigation demonstrated that the removal of the cross-lines from the tested region results in an increase of measured static mechanical properties (tensile, bending and shear). Further investigations include dynamic mechanical properties (fatigue) in regions with and without cross-lines.

Another important aspect of specimens without cross-lines is their applicability for FEM simulations. Some predictions of elastic properties were performed based on inverse laminate theory[30,31]. Microstructure of specimens without cross-lines is

equal to investigated equivalent composite structure with UD-layers[30,31]. Possible usage of specimens without cross-lines would lead to a lower deviation of the simulated properties from the experimentally validated ones and consequent higher acceptance of simulation results in future applications.

References

1. Newman B, Schäfer W. Processing and properties of oxide/oxide composites for industrial applications. In: Krenkel W, Naslain R, Schneider H, eds. *Chapter V in High temperature ceramic matrix composites*. Weinheim: Wiley – VCH Verlag GmbH; 2001: 600 – 609.

2. Ohnabe H, Masaki S, Onozuka M, Miyahara K, Sasa T. Potential application of ceramic matrix composites to aero-engine components. *Composites: Part A* 1999; 30: 489–496.

3. Zawada LP, Staehler J, Steel S. Consequence of intermittent exposure to moisture and salt fog on the high-temperature fatigue durability of several ceramic–matrix composites. *J Am Ceram Soc* 2003; 86(8): 1282–1291.

4. Prewo KM, Batt JA. The oxidative stability of carbon fibre reinforced glass–matrix composites. *J Mater Sci* 1988; 23: 523–527.

5. Mah T, Hecht NL, McCullum DE, Hoenigman JR, et al. Thermal stability of SiC fibres (Nicalon). *J Mater Sci* 1984; 19: 1191–1201.

6. Ruggles-Wrenn MB, Hetrick G, Baek SS. Effects of frequency and environment on fatigue behavior of an oxide–oxide ceramic composite at 1200°C. *International Journal of Fatigue* 2008, 30: 502–516.

7. Schmücker M, Mechnich P. All-Oxide Ceramic Matrix Composites with Porous Matrices. In: Krenkel W, editor. *Chapter 9 in Ceramic Matrix Composites*. Weinheim : Wiley – VCH Verlag GmbH; 2008: 205 – 226.

8. Schmücker M, Flucht F, Schneider H. High Temperature Behaviour of Polycrystalline Aluminosilicate Fibers with Mullite Bulk Composition. I. Microstructure and Strength Properties. *J. Eur. Ceram. Soc.* 1996; 16: 281-285.

9. Richter H, Peters PWM. Tensile strength distribution of all-oxide ceramic matrix mini-composites with porous alumina matrix phase. *J. Eur. Ceram. Soc.* 2016; 36: 3185-3191.

10. Zok FW, Levi CG. Mechanical properties of porous-matrix ceramic composites. *Adv. Eng. Mater.* 2001; 3: 15–23.

11. Holmquist MG, Lange FF. Processing and Properties of a Porous Oxide Matrix Composite Reinforced with Continuous Oxide Fibers. *J. Am. Ceram. Soc.* 2003; 86(10): 1733–1740

12. Ben Ramdane C, Julian-Jankowiak A, Valle R, et al. Microstructure and mechanical behaviour of a NextelTM610/alumina weak matrix composite subjected to tensile and compressive loadings. *J. Eur. Ceram. Soc.* 2017; 37: 2919–2932.

13. Keller KA, Jefferson G, Kerans RJ. Oxide-Oxide composites. In: Bansal NP, editor. *Chapter 16 in Handbook of Ceramic Composites*. New York City: Springer US; 2005: 377-421.

14. Kaya C, Kaya F, Butler EG, et al. Development and characterisation of high-density oxide fibre-reinforced oxide ceramic matrix composites with improved mechanical properties. *J. Eur. Ceram. Soc.* 2009; 29: 1631–1639.

15. Kostopoulos V, Loutas TH, Kontsos A, et al. On the identification of the failure mechanisms in oxide/oxide composites using acoustic emission. *NDT&E International* 2003; 36: 571-580.

16. Chawla KK. Ceramic Matrix Composites (2nd ed.). Boston: Kluwer Academic Press USA; 2003.

17. Ruggles-Wrenn MB, Radzicki AT, Baek SS, et al. Effect of loading rate on the monotonic tensile behavior and tensile strength of an oxide–oxide ceramic composite at 1200°C. *Materials Science and Engineering A* 2008; 492: 88–94.

18. Marshall DB, Evans AG. The mechanical behavior of ceramic matrix composites. *Acta Metall. Mater*. 1989; 37 (10): 2567-2583.

19. Göring J, Flucht F, Schneider H. Mechanical behavior of WHIPOX ceramic matrix composites. In: Krenkel W, Naslain R, Schneider H, eds. *Chapter V in High temperature ceramic matrix composites*. Weinheim: Wiley – VCH Verlag GmbH; 2001: 675 – 680.

20. Atkinson A, Selçuk A. Residual stress and fracture of laminated ceramic membranes. *Acta mater*. 1999; 47(3): 867-874.

21. Atkinson A, Selçuk A. Mechanical behaviour of ceramic oxygen ion-conducting membranes. *Solid State Ionics* 2000; 134: 59-66.

22. Volkmann E, Tushtev K, Koch D, et al. Assessment of three oxide/oxide ceramic matrix composites: Mechanical performance and effects of heat treatments. *Composites: Part A* 2015; 68: 19–28.

23. Heathcote JA, Gong XY, Yang JY, et al. In-plane mechanical properties of an all-oxide ceramic composite. *J Am Ceram Soc* 1999; 82(10): 2721–2730.

24. Zawada LP, Hay RS, Lee SS, et al. Characterization and high-temperature mechanical behavior of an oxide/oxide composite. *J Am Ceram Soc* 2003; 86(6): 981–990.

25. John R, Zawada LP, Kroupa JL. Stresses due to temperature gradients in ceramic–matrix-composite aerospace components. *J Am Ceram Soc* 1999; 82(1): 161–168.

26. Levi CG, Yang JY, Dalgleish BJ, et al. Processing and performance of an all-oxide ceramic composite. *J Am Ceram Soc* 1998; 81(8): 2077–2086.

27. Jurf R, Butner S. Advances in oxide–oxide CMC. *J Eng Gas Turbines Power* 2000; 122(2): 202–205.

28. Simon RA. Progress in processing and performance of porous-matrix oxide/ oxide composites. *Int J Appl Ceram Technol* 2005; 2(2) :141–149.

29. Göring J, Hackemann S, Kanka B. WHIPOX: Ein faserverstärkter oxidkeramischer Werkstoff für Hochtemperatur-Langzeitanwendungen. Materialswissenschaften und Werkstofftechnik 2007; 38(9): 766–772.

30. Shi Y, Hofmann S, Jemmali R, Hackemann S, Koch D. Determination of Elastic Properties for a Wound Oxide Ceramic Composite. *J. Ceram. Sci. Tech.* 2014; 5(1): 31-38.

31. Shi Y, Jain N, Jemmali R, et al. Prediction of Elastic Properties for a Wound Oxide Ceramic Matrix Composite Material. *Int. J. Appl. Ceram. Technol.* 2015; 12: E99–E110.

Figures

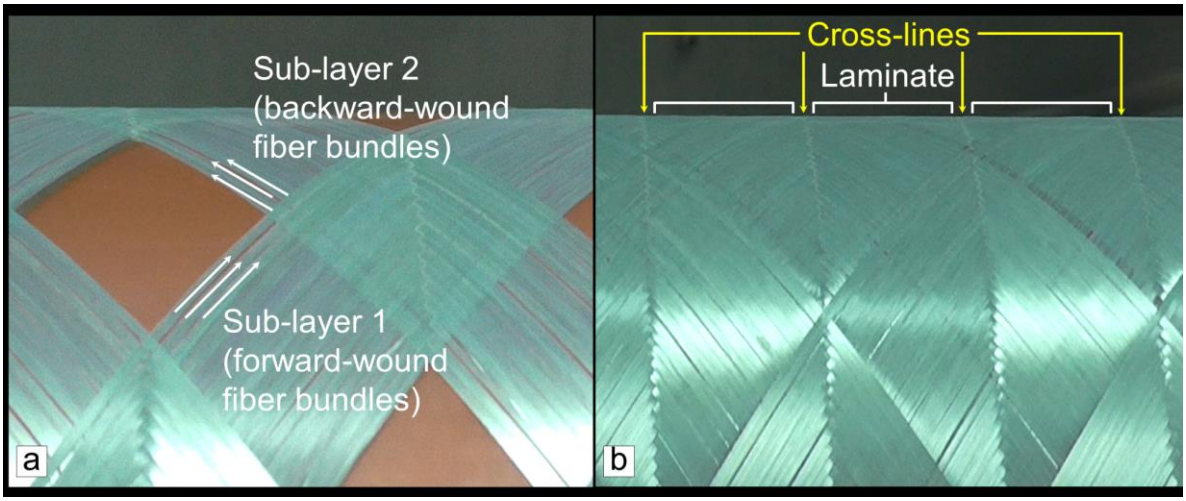

Fig. 1. Winding pattern (fiber bundles wound on a mandrel) during the winding (a) and a complete layer (100% coverage) with formed cross-lines and laminate regions (b).

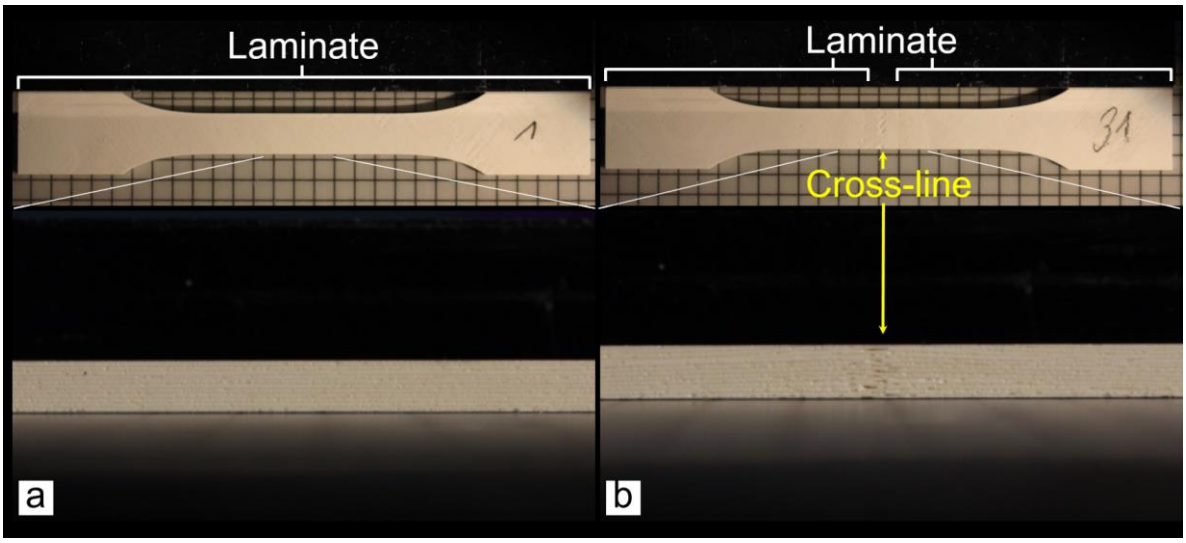

Fig. 2. Uniaxial tensile specimen without cross-lines (a) and with cross-lines in tested region (b).

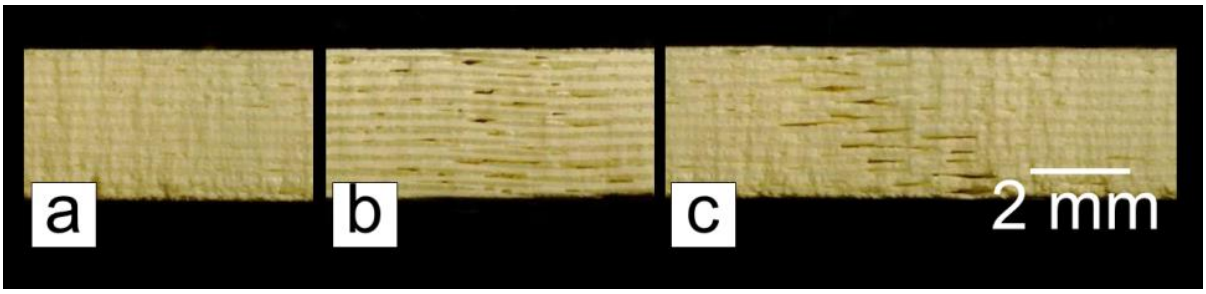

Fig. 3. WHIPOX mesostructure: laminate region without cross-lines (a), stacked cross-lines with 0°/90° fiber orientation (b) and stacked cross-lines with +45°/-45° fiber orientation (c).

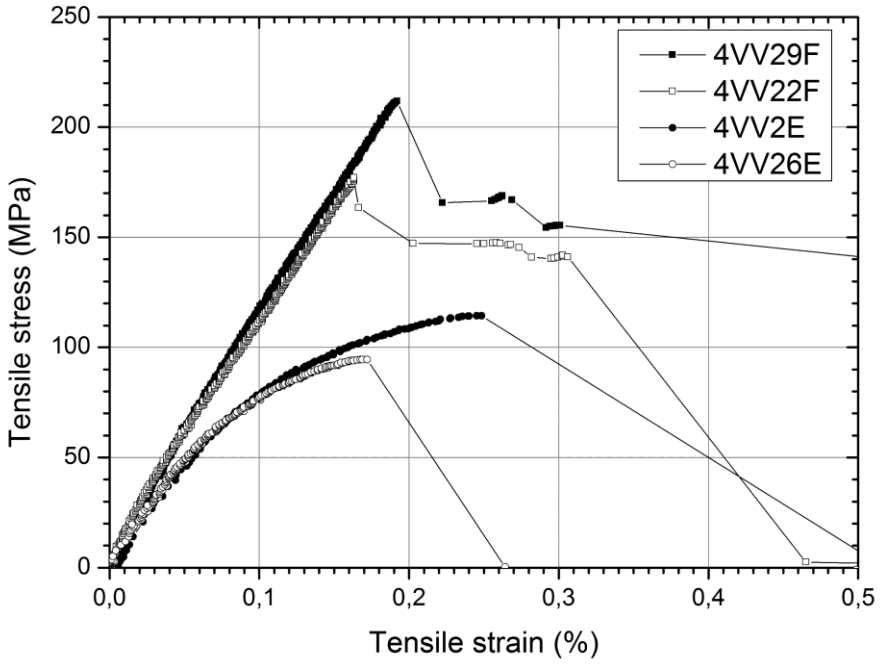

Fig. 4. Stress-strain curves of tensile samples with 0°/90° fiber orientation (laminate region 4VV29F, with a cross-line 4VV22F) and with +45°/-45° fiber orientation (laminate region 4VV2E, with a cross-line 4VV26E).

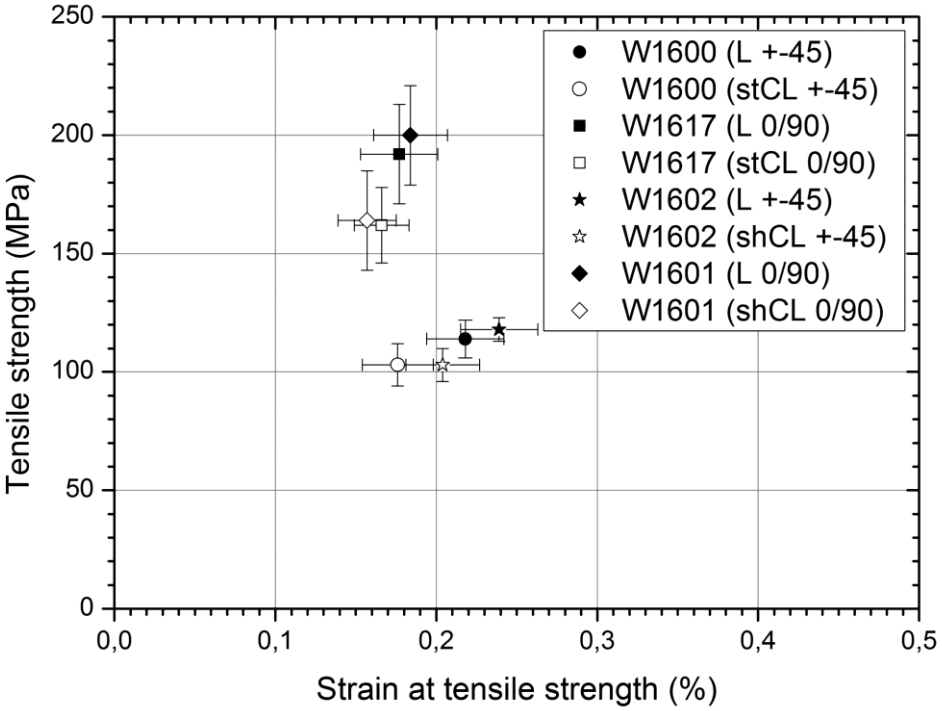

Fig. 5. Results of uniaxial tensile tests with 3 types of specimens: without cross-lines (L), with stacked cross-lines (stCL) and with shifted cross-lines (shCL).

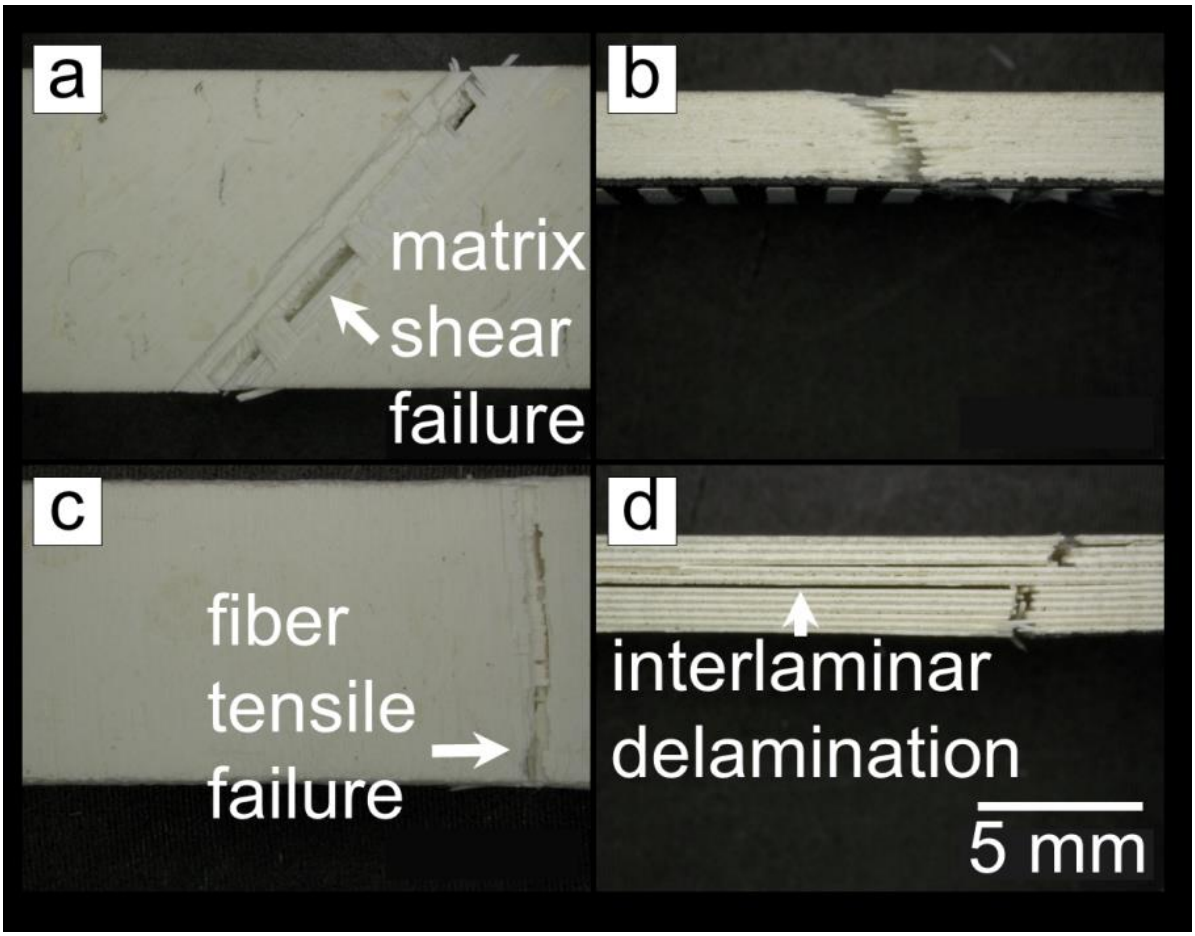

Fig. 6. Fractographic inspection of uniaxial tensile specimens without cross-lines after test: fiber orientations +45°/-45° (a,b) and 0°/90° (c,d).

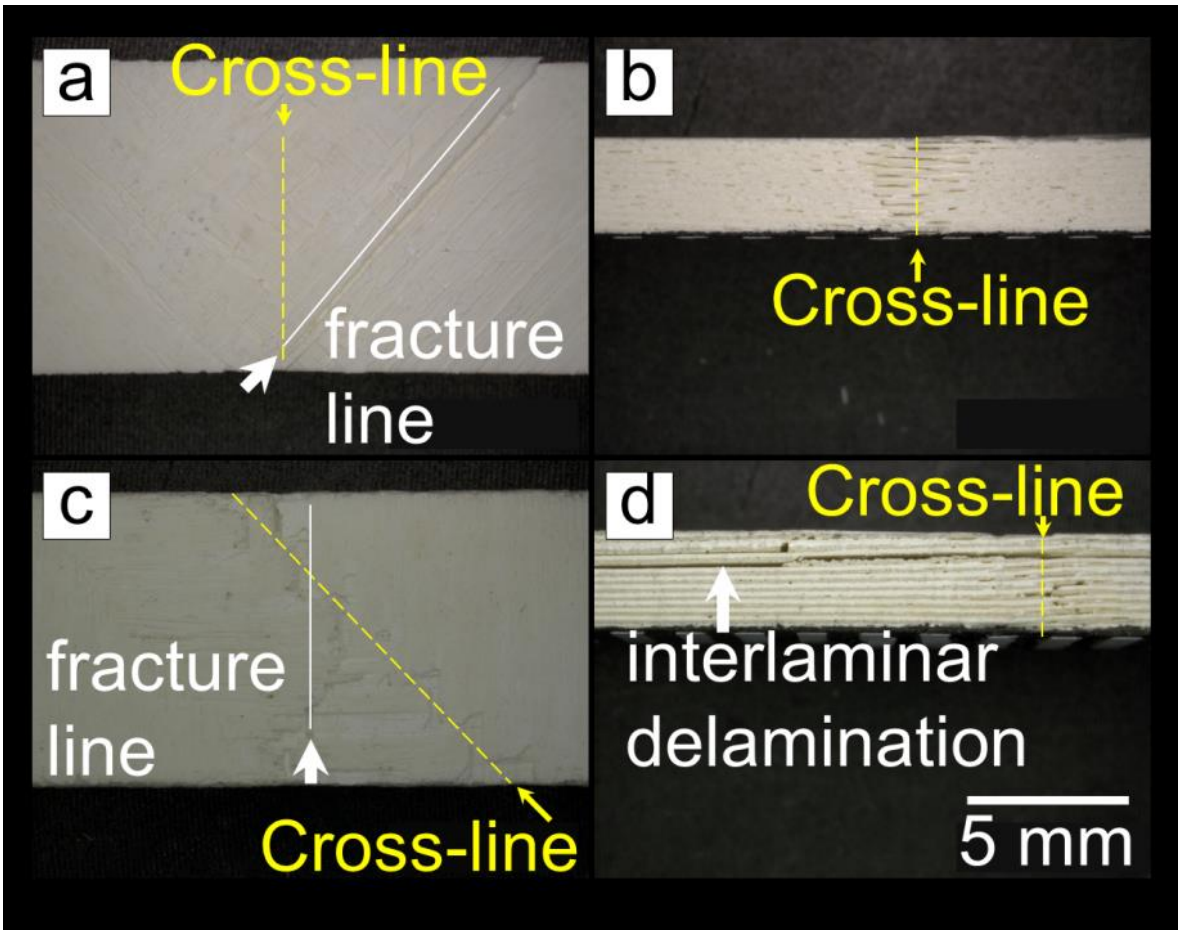

Fig. 7. Fractographic inspection of uniaxial tensile specimens with stacked cross-lines after test: fiber orientations +45°/-45° (a,b) and 0°/90° (c,d).

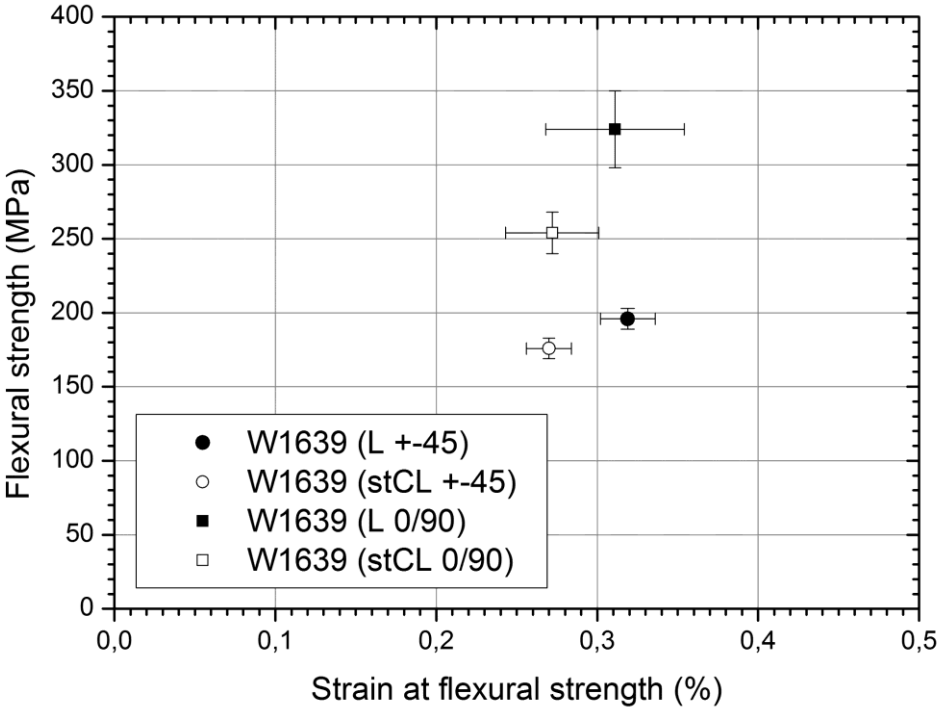

Fig. 8. Results of 4-point bending tests with 2 types of specimens (without cross-lines (L) and with stacked cross-lines (stCL)) tested with 2 fiber orientations (+45°/-45° and 0°/90°) each.

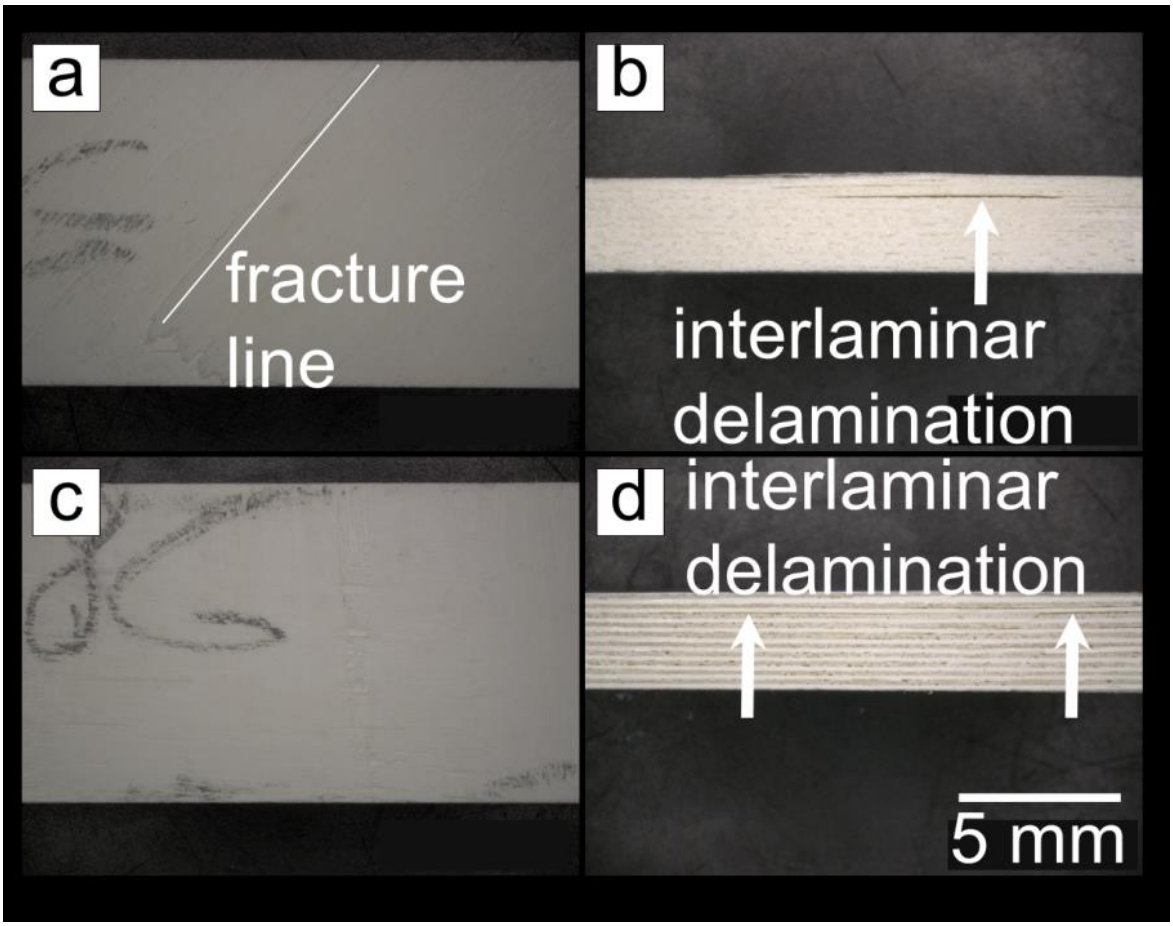

Fig. 9. Fractographic inspection of 4-point bending specimens without cross-lines after test: fiber orientations +45°/-45° (a,b) and 0°/90° (c,d).

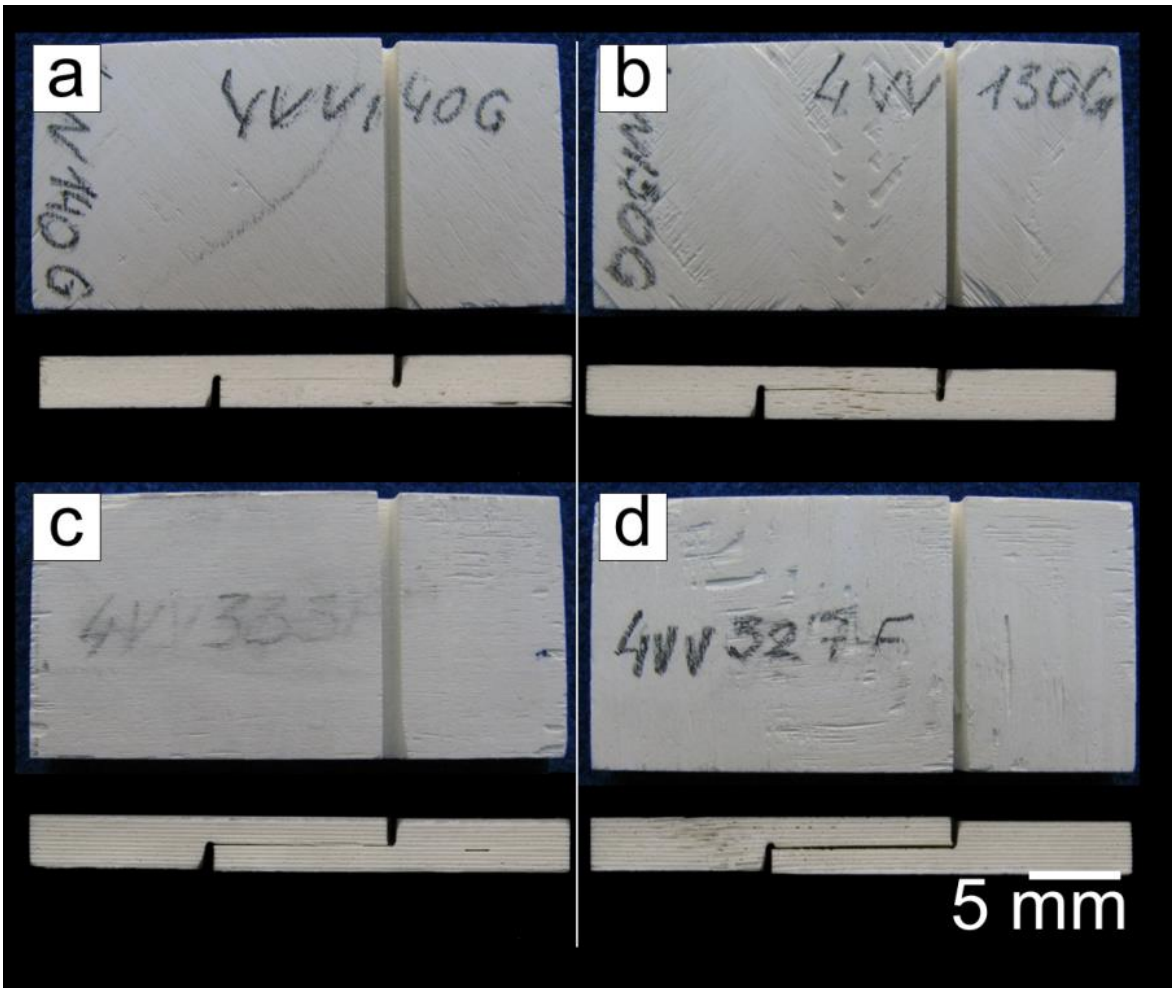

Fig. 10. Fractographic inspection of double-notch compression specimens with cross-lines (b,d) and without cross-lines (a,c) after test: fiber orientations +45°/-45° (a,b) and 0°/90° (c,d).

Tables.

Table 1. Uniaxial tensile properties (tensile strength S_U and strain at tensile strength ε_u) at ambient temperature for investigated material.

Plate (specimen fiber orientation)	Laminate	Stacked cross-lines	Shifted cross-lines
W1600 (+45°/-45°)	13 specimens:	12 specimens:	X
S_U	114 ± 8 MPa	103 ± 9 MPa	
ε_u	0.218 ± 0.024 %	0.176 ± 0.022 %	
W1602 (+45°/-45°)	15 specimens:	X	9 specimens:
S_U	118 ± 5 MPa		103 ± 7 MPa
ε_u	0.239 ± 0.024 %		0.204 ± 0.023 %
W1617 (0°/90°)	9 specimens:	9 specimens:	X
S_U	192 ± 21 MPa	162 ± 16 MPa	
ε_u	0.177 ± 0.024 %	0.166 ± 0.017 %	
W1601 (0°/90°)	10 specimens:	X	9 specimens:
S_U	200 ± 21 MPa		164 ± 21 MPa
ε_u	0.184 ± 0.023 %		0.157 ± 0.018 %

Table 2. Flexural properties (flexural strength σ and strain at flexural strength ε) at ambient temperature.

Plate (fiber orientation)	Laminate	Stacked cross-lines
W1639 (+45°/-45°)	10 specimens:	10 specimens:
σ	196 ± 7 MPa	176 ± 8 MPa
ε	0.319 ± 0.017 %	0.270 ± 0.014 %
W1639 (0°/90°)	10 specimens:	10 specimens:
σ	324 ± 26 MPa	254 ± 14 MPa
ε	0.311 ± 0.043 %	0.272 ± 0.029 %

Table 3. Interlaminar shear strength data for +45°/-45° and 0°/90° fiber-oriented double-notch compression specimens at ambient temperature.

Plate (fiber orientation)	Laminate	Stacked cross-lines
W1639 (+45°/-45°)	10 specimens:	10 specimens:
σ	7.4 ± 0.2 MPa	5.3 ± 0.6 MPa
W1619 (0°/90°)	6 specimens:	6 specimens:
σ	13.5 ± 1.4 MPa	9.7 ± 1.0 MPa